JOURNAL OF SOLID STATE CHEMISTRY 115, 55–65 (1995)

The Structures of Anhydrous Silver Sodalite $Ag_3[Al_3Si_3O_{12}]$ at 298, 623, and 723 K from Rietveld Refinements of X-Ray Powder Diffraction Data: Mechanism of Thermal Expansion and of the Phase Transition at 678 K

Peter Behrens,[1] Paul B. Kempa, Stefanie Assmann, Michael Wiebcke, and Jürgen Felsche

Fakultät für Chemie, Universität Konstanz, Postfach 5560, D-78434 Constance, Germany

Received April 8, 1993; in revised form July 5, 1994; accepted July 13, 1994

The phase transition behavior of anhydrous silver sodalite (ASS) $Ag_3[Al_3Si_3O_{12}]$ differs from that of other compounds with a sodalite structure in that the transition detected T_c = 678 K by differential scanning calorimetry does not involve the occurrence of peak splittings and/or superstructure reflections in the powder X-ray diffraction pattern of the low-temperature phase. Variable-temperature powder X-ray diffraction experiments show that the transition is from cubic to cubic and that there is a discontinuity in the thermal expansion of ASS at T_c. In order to investigate the mechanisms of thermal expansion and of the phase transition, Rietveld refinements of powder X-ray diffraction data collected at temperatures of 298, 623, and 723 K were carried out. These structure refinements show that the thermal expansion behavior between 298 K and T_c, which can be described by a quadratic function of the temperature, is determined mainly by the untilting of the sodalite framework, an experimental confirmation that a tilting mechanism is operative in the thermal expansion of sodalite frameworks. In the structures determined at 298 and 623 K, Ag^+ ions occupy positions in the center of the large windows of the sodalite cage, which are lined by six $[(Al,Si)O_4]$ tetrahedra (six-ring windows). As a consequence of the untilting, the coordination of the Ag^+ ions by framework oxygen atoms changes from a (favorable) threefold planar arrangement with Ag–O bond lengths d_{Ag-O} of 2.347(5) Å at 298 K to an (unfavorable) environment with six O neighbors arranged in a plane at longer distances (d_{Ag-O} = 2.50(1) Å (3×) and 2.79(1) Å (3×)) at 623 K. At 723 K, above T_c, the Ag^+ ions have been shifted away from the center of the six-ring window, allowing the framework to collapse. Then, Ag^+ is again in a threefold oxygen coordination (d_{Ag-O} = 2.375(6) Å) with silver at the apex of a flat trigonal $[AgO_3]$ pyramid. The occurrence of the phase transition can be rationalized by the demand of the Ag^+ ion for small coordination numbers and short, covalent bonds and thus probably is a consequence of the specific bonding characteristics of the Ag^+ ion.

[1] To whom correspondence should be addressed at present address: Institut für Anorganische Chemie, Ludwig-Maximillians-Universität München, Meiserstrasse 1, D-80333 München, Germany.

INTRODUCTION

Sodalites are aluminosilicate framework structures which contain guest complexes of cations A and/or an anion X and/or water in their cages. In the case of a monovalent anion X the general formula is:

$$[A_{3+x}X_x(H_2O)_n][Al_3Si_3O_{12}].$$

The framework of sodalites is built from corner-sharing AlO_4 and SiO_4 tetrahedra arranged to give a space-filling assembly of so-called sodalite or β-cages with the shape of a $[4^66^8]$ truncated octahedron. The maximum aperture of these cages is a window lined by six $[(Al,Si)O_4]$ tetrahedra (six-ring window). As typical host–guest compounds, sodalites often show phase transitions (1) which are usually due to orientational ordering processes of the guest species at lower temperatures; this orientational ordering may be transmitted to changes in the positions of the framework atoms. At higher temperatures, the guest species are dynamically disordered over several equivalent orientations. Corresponding orientational order–disorder phase transitions were observed in aluminosodalites with A = Na and different anions X (2, 3), as well as in compounds with the sodalite structure possessing other framework compositions (3–10). Order–disorder processes are also believed to be responsible for the phase transitions observed in anion-free anhydrous sodalites (3) $[A_3\square][Al_3Si_3O_{12}]$ with A = Li^+, Na^+, K^+; here, it is assumed that three nonframework cations A order on the four available, tetrahedrally disposed sites ($\square$ signifies the vacant site). A typical signature of these types of order–disorder phase transitions in sodalites is the change from cubic symmetry in the high-temperature form to lower crystal symmetry in the low-temperature form, leading to peak splitting and/or superstructure reflections in the diffractograms of the low-temperature

0022-4596/95 $6.00

form. There is currently great interest in these phase transitions, not only from basic research trying to unravel the intriguing host–guest interactions guiding the ordering behavior, but also from applied zeolite chemistry, where the host–guest structural interactions in sodalites serve as a model case for the even more complex processes occurring in zeolites during sorption and catalytic reactions.

From hydrothermal synthesis, the nonframework cation A in aluminosilicate sodalites is Na^+. By ion-exchange from aqueous $AgNO_3$ solutions or from the melt, Na^+ ions can be replaced by Ag^+ ions (11–15). The regular void structure of sodalites can thus be used for the controlled assembly of small aggregates of silver I-VII semiconducting compounds leading to so-called "semiconductor quantum supralattices" in the case of halide sodalites (12–18) or to "expanded Ag metal" produced by intracage reduction of enclathrated silver oxalate (13, 19). Interesting photosensitivities and redox reactivities make silver sodalites potentially useful for applications in, e.g., optoelectronic image processing and as optical data storage materials (13, 18–20). We have concentrated our investigations on silver hydrosodalites (11, 21) of the general formula $[Ag_{3+x}(OH)_x(H_2O)_n][Al_3Si_3O_{12}]$, especially in order to compare the compounds occurring in this system to those that exist in the sodium hydrosodalite system, which we have studied extensively in the years before (22). The main result of these studies (21) is a strong similarity in the possible compositions of pure compounds, and in their dehydration and rehydration behavior.

Important differences were found, however, in the structures of the fully hydrated sodalites $[Na_3(H_2O)_4][Al_3Si_3O_{12}]$ (23) and $[Ag_3(H_2O)_4][Al_3Si_3O_{12}]$ (24) and, to be reported here, in the phase transition behavior of the anhydrous sodalites $[A_3\square][Al_3Si_3O_{12}]$. For $A^+ = Na^+$, a phase transition from a cubic high-temperature phase to a low-temperature phase of lower crystallographic symmetry, signified by peak splittings in the X-ray diffractogram, is observed at 523 K (3). Although the structure of the low-temperature phase has not been determined yet, we tentatively assume that the phase transition involves ordering of the three Na^+ cations over the four sites available per cage. In the case of ASS, $Ag_3[Al_3Si_3O_{12}]$, we found a phase transition at a temperature of $T_c = 678$ K by differential scanning calorimetry (DSC) measurements. On variable temperature powder X-ray diffraction photographs, neither peak splitting nor the appearance of additional reflections were observed; at any temperature between 298 and 1100 K the diffraction pattern can be indexed on a cubic unit cell. The absence of peak splittings and superstructure reflections in the low-temperature phase of ASS differentiates this phase transition from the phase transitions observed in anhydrous sodium sodalite and in anion-bearing sodalites. A detailed analysis of the variable temperature X-ray diffraction photographs revealed a discontinuity in the thermal expansion of ASS at T_c.

In order to elucidate the mechanism of thermal expansion and the nature of the phase transition in $Ag_3[Al_3Si_3O_{12}]$, we performed Rietveld refinements of powder X-ray diffraction data taken at 298, 623 (i.e., about 50 K below the phase transition temperature) and at 723 K (i.e., about 50 K above the phase transition temperature).

2. EXPERIMENTAL

ASS was prepared via a four-step procedure involving synthesis of basic sodium hydrosodalite in Teflon-lined steel autoclaves (22), Soxhlet extraction of NaOH with water at 373 K to give nonbasic sodium hydrosodalite (22), and subsequent ion-exchange with a 1 N $AgNO_3$ solution at 383 K in an autoclave (21). Dehydration of the resulting nonbasic silver hydrosodalite (SHS) $[Ag_3(H_2O)_4][Al_3Si_3O_{12}]$ by heating to 623 K for about 6 hr *in vacuo* gives ASS (21):

$$[Na_4(OH)(H_2O)][Al_3Si_3O_{12}] \xrightarrow[-NaOH]{+H_2O}$$

$$[Na_3(H_2O)_4][Al_3Si_3O_{12}] \xrightarrow[-Na^+]{+Ag^+}$$

$$[Ag_3(H_2O)_4][Al_3Si_3O_{12}] \xrightarrow[-H_2O]{} [Ag_3][Al_3Si_3O_{12}].$$

ASS possesses an off-white color, which is probably due to a small amount of finely dispersed silver formed by autoreduction involving partial disintegration of the sodalite framework (see below). Due to its extreme hygroscopicity, ASS was produced by *in situ* dehydration of SHS for all the measurements described below (21).

DSC measurements were performed on a Perkin–Elmer DSC-7 apparatus using a heating rate of 10 K/min. The sample of SHS, kept in an aluminium pan, was dehydrated on the calorimeter and then cycled through the phase transition several times. For enthalpy measurements, the calorimeter was calibrated by measuring the melting enthalpy of metallic indium.

Variable-temperature X-ray powder diffraction photographs were taken in order to follow changes in the lattice constant a of ASS. A home-built heating camera employing Guinier geometry and Cu$K\alpha_1$ radiation was used in the step-scan mode. The sample of SHS and a small amount of Au for 2θ calibration were placed in a quartz capillary. After dehydration on the heating camera, diffraction patterns were recorded for 6 hr each in steps of 5 K in a temperature region of ± 50 K around the phase transition temperature of 678 K and with larger step widths at other temperatures between 298 and 1100 K.

Cubic lattice constants a were determined after calibration by least-squares refinement from the positions of 17 sodalite reflections occurring between 10° and 75° 2θ.

For the measurement of X-ray powder diffraction patterns suitable for Rietveld refinement, SHS was transferred to a Scintag PAD-X powder diffractometer equipped with a Bühler heating device. After evacuation of the heating chamber, a full diffraction profile of SHS was taken using Cu$K\alpha$ radiation. Results of the refinement of this pattern are given elsewhere (24). The sample was then heated to 623 K and kept at this temperature for 12 hr to achieve full dehydration. A diffraction pattern of ASS, subsequently named ASS-623, was taken at this temperature. A pattern of the high-temperature form was measured after heating to 723 K (ASS-723); after cooling to room temperature, the ASS-298 pattern was recorded. The measurement of the patterns took about 22 hr each. Further details of the measurements are given in Table 1.

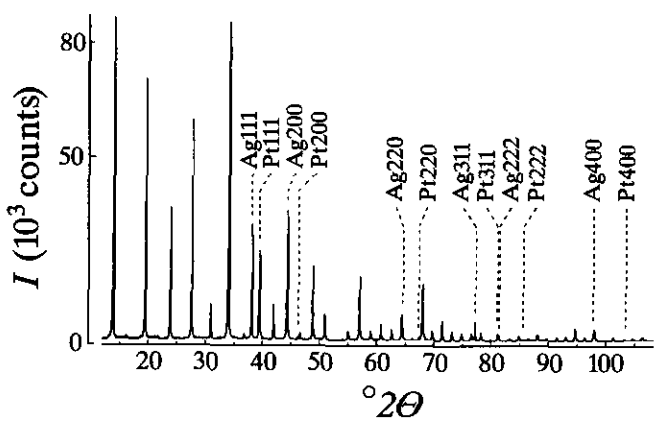

FIG. 1. X-ray powder pattern of anhydrous silver sodalite at 298 K after background subtraction (Szintag diffractometer, ASS-298 data set). The reflections of Ag (from partial destruction of the sodalite compound) and Pt (from the sample holder) are indicated. For Rietveld refinement, these reflections were deleted from the pattern.

Inspection of the three diffraction patterns revealed the presence of reflections from the face-centered cubic lattices of elemental Pt and Ag (Fig. 1.). The Pt reflections stem from the sample holder. The Ag reflections are not present in the pattern of SHS but their intensity increases with prolonged heating time of the ASS sample; the formation of elemental Ag is due to a slow disintegration of ASS at elevated temperatures, probably by the process of autoreduction that has been observed in silver-exchanged zeolite A samples, too (see, e.g., Refs. 25–28). Those 2θ regions where strong X-ray reflections from Ag and Pt occur were eliminated before the Rietveld refinements. Due to the fact that the amount of disintegration is small, no further ill effects on the refinements were encountered. It was possible to use the positions of the Ag reflections for calibration of the 2θ scale. Cubic lattice constants derived after this calibration by the least-squares refinement of the sodalite reflections showed better

TABLE 1
Crystallographic Data

Data set	ASS-298	ASS-623	ASS-723
Data collection temperature (K)	298	623	723
Profile range (°2θ)	12.0–108.9	12.0–108.3	12.0–109.4
Step scan increment (°2θ)	0.02	0.02	0.02
Count time per step (sec)	20	20	20
Standard peak for peak shape function hkl	200	200	200
for °2θ region (°2θ)	12.0–21.0	12.0–23.0	12.0–23.0
Standard peak for peak shape function hkl	422	310	211
for °2θ region (°2θ)	21.0–108.9	23.0–108.3	23.0–109.4
Space group; Z	$P\bar{4}3n$; 2	$P\bar{4}3n$; 2	$Pm\bar{3}n$; 2
a(Å)	9.122(2)	9.142(2)	9.158(2)
Number of observations	4294	4265	4167
Number of contributing reflections	99	99	100
Number of structural parameters	9	9	9
Number of profile parameters	7	7	7
Statistically expected R_{exp}	0.086	0.104	0.102
R_{wp}	0.125	0.147	0.148
R_F	0.066	0.128	0.101
Residual electron density (e/Å^3)	2.38	2.71	1.89
at x	0.25	0.102	0.25
y	0	0.102	0
z	0.5	0.102	0.5

agreement with the parameters calculated from the variable-temperature X-ray diffraction photographs than the lattice constants emerging from the Rietveld refinements, indicating that possible errors, for example, sample movement due to heating, are not adequately accounted for by the Rietveld refinement procedure. In Table 1, a values obtained after the calibration on the Ag reflections are given.

Data reduction proceeded by estimating background intensities in regions between well-separated peaks and by employing a linear interpolation to obtain the background correction. The $K\alpha_2$ component of the reflections was eliminated using the procedure of Laddell *et al.* (29). For each data set, two peaks were selected and standard peak profile functions were calculated. One peak was used for the refinement in the low 2θ region and the other in the high 2θ region (for details see Table 1). Then, the whole profile was analyzed for the dependence of peak width and peak asymmetry on 2θ. Seven profile parameters (one for the lattice constant, two for the correction of the 2θ scale, and four for the 2θ dependence of the peak width and of the peak asymmetry) were refined and applied to the experimental profile. Since the crystallites were almost spherical, no problems from the preferred orientation arose. Atomic scattering factors (uncorrected for anomalous dispersion) for neutral atoms were used for Al, Si, and O; for silver the scattering factor of Ag^+ was used. Further details of the data reduction are also collected in Table 1.

A comparison of the peak widths of selected reflections from the three diffraction patterns showed no anomalies. An anomalous broadening of the peaks of the ASS-623 and the ASS-298 patterns would occur if the true symmetry of the low-temperature phase of ASS was lower than cubic and if the lattice parameters were so nearly cubic that their differences were too small to lead to peak splitting. Absence of anomalous peak broadening is thus in agreement with a transition involving cubic symmetry in both phases.

The X-ray Rietveld System XPS-82 (30) was used for the refinement of all three structures. To facilitate convergence in the early stages of the refinements, geometric constraints were applied to bond distances and angles of the framework atoms. As the refinements proceeded, these constraints were given less and less weight until they were finally removed. In the last cycle of successful refinements, all parameter shifts were smaller than 1% of their esd's.

Starting parameters for the ASS-298 pattern were taken from the refinement of $Na_3[Al_3Si_3O_{12}]$ at 675 K (23). Silver ions were thus placed on the 8*e* position in space group $P\bar{4}3n$. The population parameter was initially fixed to 0.75 corresponding to three Ag^+ per cage. Unfixing in later stages of the refinement resulted in no significant deviations from 0.75. So, it was decided to keep this value fixed in order to limit the number of refined parameters. For the same reason, the isotropic thermal parameters for the tetrahedral framework atoms Al and Si were assumed to be equal in all refinements.

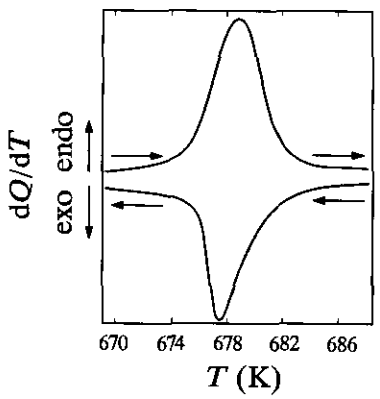

FIG. 2. Differential scanning calorimetry traces of anhydrous silver sodalite. Heating and cooling is indicated by arrows. Sample mass, 337 mg; heating rate, 10 K/min; atmosphere, N_2.

RESULTS

Differential Scanning Calorimetry

The DSC curve shown in Fig. 2 reveals that the transition from the low- to the high-temperature phase occurs at a temperature of $T_c = 678 \pm 3$ K (peak maximum, standard deviation from several measurements on different samples). The transition is reversible and shows only a small hysteresis. A transition enthalpy of $\Delta H = 7.1$ kJ/mole was measured.

X-Ray Heating Experiments

The temperature dependence of the cubic lattice parameter $a = f(T)$ is shown in Fig. 3. The reason for the large difference in the a_0 values determined at 298 K—9.100(5) Å from the Guinier pattern and 9.122(2) Å from the ASS-298 data set—is not known. Between 298 K and T_c the thermal expansion can be described as quadratic according to the equation $a = a_0(1 + AT + BT^2)$ with the parameters $a_0 = 9.101$ Å, $A = 3.5 \times 10^{-6}$°C^{-1}, $B = 17.9 \times 10^{-9}$°C^{-2}. The parameters stem from a fit to the data between 298 and 648 K. The temperature T is in °C here to facilitate comparison with the similar relationships described by Henderson and Taylor (31), who also observed quadratic expansion behavior for several sodalites with room temperature lattice constants larger than 9.05 Å. A mean linear thermal expansion coefficient $\alpha = \Delta a/(a_0 \cdot T)$ of $10.4(5) \times 10^{-6}$ K^{-1} calculated for the tempera-

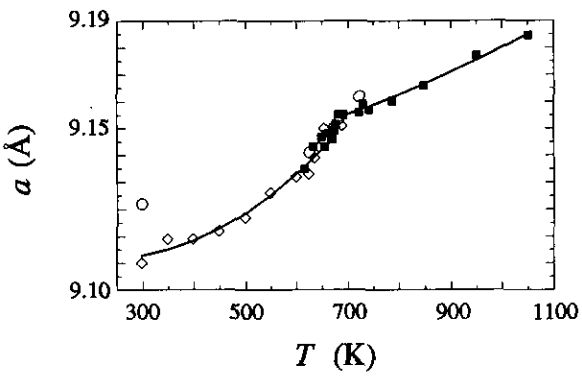

FIG. 3. Cubic lattice constant a as a function of temperature. Open squares denote data points obtained during cooling; full squares denote those measured during heating (variable-temperature X-ray Guinier camera). Open circles correspond to lattice constants refined on the basis of the data sets used for Rietveld refinements.

ture region 298–648 K fits well to the relation between α and a_0 found by Henderson and Taylor (see Fig. 3 of ref. 31). In difference to the discontinuities described by these authors for iodide and for sulfate-containing sodalites, where the expansion above the phase transition is linear, the thermal expansion of ASS above T_c seems to be quadratic, too, although the quadratic term is less important here: Parameters refined to $a_0 = 9.141$ Å, $A = 0.5 \times 10^{-6}°C^{-1}$, $B = 6.8 \times 10^{-9}°C^{-2}$ for the data points between 698 and 1073 K.

Rietveld Refinement of Anhydrous Silver Sodalite at 298 K

In $P\bar{4}3n$, the refinement of the ASS-298 pattern with isotropic thermal parameters initiated on the results of the refinement of $Na_3[Al_3Si_3O_{12}]$ at 675 K (23) proceeded to R values of $R_F = 0.102$ and $R_{wp} = 0.150$. Inspection of the difference profile showed substantial deviations of the calculated intensities from the measured ones especially at high diffraction angles. Difference Fourier synthesis revealed substantial residual electron density of about 3.3 e/Å^3 at x, x, x (8e) positions neighboring the Ag position. It was therefore decided to refine the silver ion with anisotropic thermal parameters. The refinement then converged at substantially lower R values ($R_F = 0.066$ and $R_{wp} = 0.125$). The strongest residual electron density in the difference Fourier map is now located at the position of the framework atom A1 (2.4 e/Å^3).

Crystallographic details are summarized in Table 1, and the final parameters in Table 2. Selected bond distances are given in Table 3, together with other geometric parameters that will be discussed later. The measured, calculated and difference profiles are shown in Fig. 4a. The geometry of a sodalite cage is shown in Fig. 5. Silver ions occupy the centers of four tetrahedrally disposed six-ring windows with a population of 0.75. Details of the siting of the Ag ion in the six-ring window of the sodalite framework are provided in Fig. 6a.

Rietveld Refinement of Anhydrous Silver Sodalite at 623 K

Starting parameters for the refinement of the ASS-623 pattern were taken from the preceding refinement of

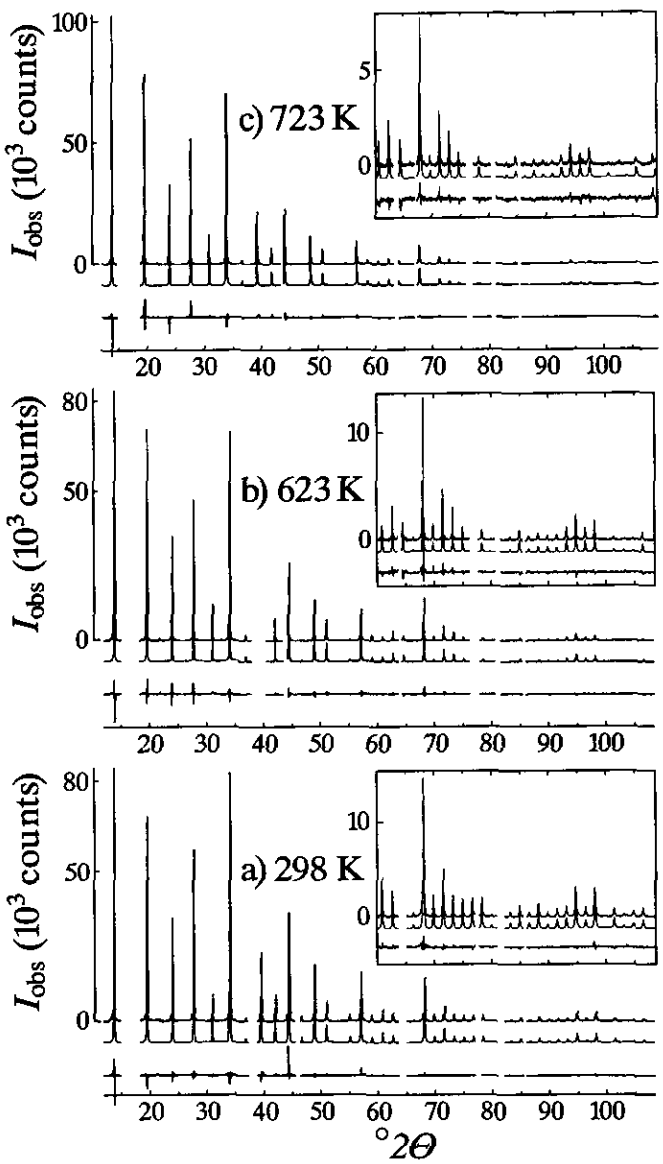

FIG. 4. Diffraction profiles from the Rietveld refinements of the three data sets: (a) 298 K, (b) 623 K, (c) 723 K. Top, experimental profile; center, calculated profile; bottom, difference profile. The insets show the regions between 60°2θ and 108°2θ on an enlarged intensity scale.

TABLE 2
Sites, Atomic Positional Parameters, Thermal Parameters U, and their esd's in Parentheses

Data set	ASS-298	ASS-623	ASS-723
Data collection temperature (K)	298	623	723
Space group	$P\bar{4}3n$	$P\bar{4}3n$	$Pm\bar{3}n$
Si	6*c*	6*c*	6*d*
Position Site symmetry	$\bar{4}$	$\bar{4}$	$\bar{4}m2$
x	0.25	0.25	0.25
y	0.5	0.5	0.5
z	0	0	0
U(Å²)	0.0051(3)	0.0067(5)	0.0387(7)
Al	6*d*	6*d*	6*c*
Position Site symmetry	$\bar{4}$	$\bar{4}$	$\bar{4}m2$
x	0.25	0.25	0.25
y	0	0	0
z	0.5	0.5	0.5
U(Å²)	0.0051(3)	0.0067(5)	0.0387(5)
O	24*i*	24*i*	48*l*
Position Site symmetry	1	1	1
x	0.1398(8)	0.142(9)	0.1456(8)
y	0.1470(8)	0.149(9)	0.1506(8)
z	0.4583(3)	0.480(1)	0.4642(3)
U(Å²)	0.003(1)	0.034(1)	0.045(1)
Occupancy	1.000	1.000	0.500
Ag	8*e*	8*e*	16*i*
Position Site symmetry	3	3	3
x	0.2426(1)	0.2438(4)	0.2303(3)
y	*x*	*x*	*x*
z	*x*	*x*	*x*
U_{11}(Å²)[a]	0.0334(4)	0.067(1)	0.039(1)
U_{12}(Å²)[a]	0.0225(5)	0.043(1)	0.017(2)
Occupancy	0.750	0.750	0.375

[a] Definition of U_{ij} according to $f \sim \exp\{-2\pi^2(h^2a^{*2}U_{11} + 2hka^*b^* \cos\gamma^* U_{12} + \ldots)\}$.

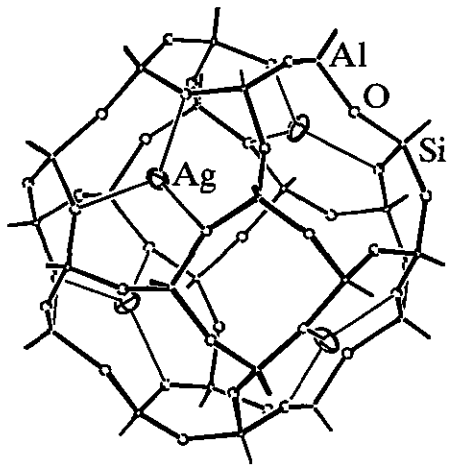

FIG. 5. Structure of a sodalite cage of anhydrous silver sodalite as determined from the refinement of the ASS-298 data set. Ag^+ ions are drawn with their thermal ellipsoids, oxygen atoms as large and framework Al and Si atoms as small circles.

ASS-298. The refinement stopped at R values of R_F = 0.128 and R_{wp} = 0.147. Compared to the other refinements, the analysis of the ASS-623 pattern proceeded less smoothly and the parameters indicating the quality of the refinement, especially the esd values, were worse. Another strong indication for the restricted reliability of this refinement are the rather short Al–O and Si–O distances (see Table 3). The weakness of the ASS-623 data set may be due to a small amount of residual water molecules in the cages (incomplete dehydration of the sample; compare the sequence of measurements described under Experimental). The position of highest residual electron density in the difference Fourier synthesis (x, x, x with x = 0.102, Table 1) corresponds to the position of an H_2O-oxygen atom in the silver hydrosodalite $[Ag_3(H_2O)_4][Al_3Si_3O_{12}]$ (24). Nevertheless, by applying due care in the interpretation of the ASS-623 data, these will not be excluded from the discussion. Indeed, evidence that the

results are essentially correct is provided by the fact that they fit well into the scenario developed for the thermal expansion and phase transition behavior of ASS, as will be demonstrated in the discussion.

Crystallographic details are again summarized in Table 1, final parameters in Table 2, and selected bond distances in Table 3. The profile plots are shown in Fig. 4b. Details of the sitting of the Ag ion in the six-ring window are shown in Fig. 6b.

Rietveld Refinement of Anhydrous Silver Sodalite at 723 K

The attempt to refine the ASS-723 pattern using the results of ASS-623 as initial parameters in space group $P\bar{4}3n$ lead to strong residual electron densities at the position of the framework *Al* atom (5.0 e/Å^3) and near to the Ag^+ ion (3.8 e/Å^3 at 0.236, 0.234, 0.234). *R* values were $R_f = 0.152$ and $R_{wp} = 0.152$ and $R_{wp} = 0.127$ and some constraints on bond distances and angles of the framework had to be active, otherwise the refinement diverged. Obviously, the high-temperature form of ASS possesses substantial structural differences to the low-temperature form. Especially with regard to the position and/or the dynamic motion of the silver ion, changes must occur that cannot be described further by anisotropic thermal displacement parameters. We therefore decided to split the Ag position to two 8*e* positions. These refined to positional parameters *x* of 0.225 and 0.265, respectively, with an occupation of 0.375 each. Nevertheless, this refinement in space group $P\bar{4}3n$ still did not progress smoothly, and it was not possible to release all constraints. *R* values were $R_F = 0.127$ and $R_{wp} = 0.159$. Based on crystallographic considerations, we changed to the centrosymmetric space group $Pm\bar{3}n$, a minimal supergroup of $P\bar{4}3n$ with the same reflection conditions. In $Pm\bar{3}n$, Ag^+ ions are located in position 16*i* with a population of 0.375; O atoms were ascribed to the general position 48*l* with a population of 0.5. This model implies positional disorder of the Ag and O atoms. In total, it possesses the same number of variable structural parameters as the $P\bar{4}3n$ models of the analyses of the ASS-298 and ASS-623 data sets. Refinement proceeded smoothly in $Pm\bar{3}n$, leading, after the release of all constraints, to *R* values of $R_F = 0.101$ and $R_{wp} = 0.148$. The strongest residual electron density observed at the position of the Al framework atom dropped from 3.9 e/Å^3 in the $P\bar{4}3n$ model with two 8*e* Ag positions to 1.9 e/Å^3 in the $Pm\bar{3}n$ case. To further test the choice of the correct

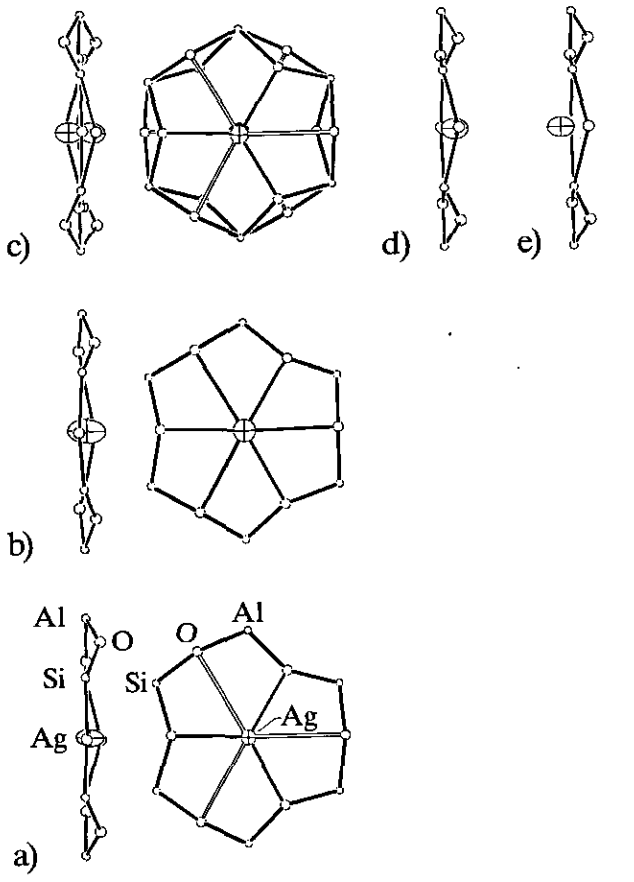

FIG. 6. The coordination of Ag and the conformation of the six-ring window of the framework as determined from the refinement of the (a) ASS-298, (b) ASS-623, (c) ASS-723 refinement; (c) is a superposition of all positions of silver and oxygen atoms obtained in this refinement; (d) and (e) show the two different Ag coordinations that can be derived from these positions (see text).

TABLE 3
Selected Bond Distances and Angles

Data set		ASS-298	ASS-623	ASS-723
Si–O	(Å)	1.628(7)	1.59(1)	1.646(7)
Al–O	(Å)	1.718(7)	1.69(1)	1.708(8)
O–Si–O	2 × (°)	109.5(3)	109.8(8)	112.9(4)
	4 × (°)	109.4(9)	109.3(3)	107.7(3)
O–Al–O	2 × (°)	108.4(3)	108.6(8)	112.0(3)
	4 × (°)	110.0(2)	109.8(7)	108.2(3)
Si–O–Al	(°)	148.9(3)	157(1)	149.3(3)
Ag–O	(Å)	2.347(5)	2.50(1)	2.375(6)
		2.981(5)	2.79(1)	2.899(6)
				2.390(6)
				2.991(6)
O ... O[a]	(Å)	4.082(8)	4.31(1)	4.090(8)
φ_{Si}[b]	(°)	16.7	8.3	14.0
φ_{Al}[b]	(°)	15.8	7.3	13.6
α_{Si}[c]	(°)	109.6	110.3	112.9
α_{Al}[c]	(°)	108.4	108.9	112.0
a[c]	(Å)	9.122	9.142	9.158

Note. esd's in parentheses as well as the values of φ, α and *a* calculated from the coordinates of the oxygen atoms according to Ref. (42) and (40), respectively.

[a] Shortest O ··· O distance across the six-ring window.

[b] Calculated according to (42).

[c] Calculated according to (40).

model, we adopted the $Pm\bar{3}n$ model as a starting point for the refinements of the ASS-298 and ASS-623 data. These attempts were not successful.

A similar problem, the presence of several neighboring Ag positions on the body diagonal of a cubic unit cell, arose during the structure refinements of silver zeolite *A*. Whereas Kim and Seff (25) used strongly elongated displacement ellipsoids to describe the corresponding electron density, Gellens *et al.* (32–34) preferred to use several partly occupied positions. Due to the results of the extensive cross-checking of the different models with the data sets, we believe that the crystallographic description of ASS at 723 K in space group $Pm\bar{3}n$ is the most appropriate.

Crystallographic details for the $Pm\bar{3}n$ refinement are summarized in Table 1, the final parameters in Table 2, and selected bond distances in Table 3. The profile plots are given in Fig. 4c. Details of the siting of the Ag^+ ion in the six-ring window are shown in Fig. 6c to 6e and will be explained further in the Discussion.

4. DISCUSSION

The Coordination of the Silver Ions

The essential features of the coordination of the Ag^+ ions in the three structures are shown in Fig. 6. In the low-temperature phase (Fig. 6a), silver ions occupy positions very close to the center of the six-ring (the center is located at 0.25, 0.25, 0.25). Note that in contrast to silver zeolite A (25, 34), no intrazeolitic cluster formation takes place during dehydration. Ag^+ ions that are reduced to Ag atoms during the thermal treatment obviously prefer to form a separate phase of elemental Ag (see Fig. 1 and Experimental).

The framework conformation at 298 K leads to a trigonal-planar coordination of Ag^+ by oxygen atoms (Figs. 5 and 6a) with a distance d_{Ag-O} = 2.347(5) Å (full Ag–O sticks in Figure 6a). The three other oxygen atoms of the six-rings are at a nonbonding distance of 2.981(5) Å (open Ag–O sticks in Fig. 6a). This three fold coordination is very similar to that observed for the majority of silver ions in silver zeolite *A* (34), where d_{Ag-O} = 2.27–2.30 Å. Silver typically adopts low coordination numbers, especially in oxide compounds. Although linear coordination is even more common, threefold coordination is observed, for example, in silver disilicate $Ag_6Si_2O_7$ (35), in $(Ag_4SiO_4)_2 \cdot AgNO_3$ and its germanate analogue $(Ag_4GeO_4)_2 \cdot AgNO_3$ (36), in $AgBO_2$ (37), and in $Ag_5Pb_2O_6$ (38). Typical Ag–O bond lengths range from 2.16–2.42 Å with a mean value around 2.30 Å, which compares well with the 2.347 Å found in ASS at 298 K. In most of these cases of threefold coordination, however, the Ag^+ ion is located above and not in the center of the triangle formed by the coordinating oxygen atoms, *i.e.*, the $[AgO_3]$ unit forms a flat trigonal pyramid with Ag at the apex. The tendency of Ag^+ to adopt small coordination numbers has been traced back to an appreciable amount of covalent bonding between silver and oxygen. AgL_3 XANES spectra of ASS show that the Ag^+ ions are bonded to the framework oxygen atoms with bonds of medium covalent character (39). This is in agreement with the threefold coordination and the observed bond distance.

At 623 K the value of the single positional parameter x of the Ag^+ has not changed significantly from that of the ASS-298 refinement. There is a drastic change, however, in the coordination of Ag^+ due to a change in the conformation of the framework. So, 50 K below the transition temperature, the silver atoms are in an extremely unusual coordination environment, namely the center of a nearly planar ring of six oxygen atoms, three at a distance of 2.50(1) Å and three at an only slightly longer distance of 2.79(1) Å (Fig. 6b). This unusual coordination is dictated by the framework conformation and is a consequence of the untilting of the framework.

The preferred direction of the thermal motion of the silver ions is along the ⟨111⟩ directions of the cubic cell, *i.e.*, perpendicular to the plane of the six-ring window for all refined structures. At 298 K, the values of the corresponding root mean square amplitudes (RMS) of the displacement rotational ellipsoid are 0.28 Å parallel and 0.10 Å vertical to the principal axis. Our refinements reflect the increased thermal motion by a 50% increase of the values of the thermal parameters on going from 298 to 623 K (Table 2). The RMS values have increased to 0.39 (parallel) and 0.16 (vertical) at 623 K. It is interesting to note that the ratio $RMS_{\parallel}/RMS_{\perp}$ is the same for both structures of the low-temperature phase.

The structure of ASS at 723 K is characterized by the positional disorder of the Ag^+ ions and the O framework atoms. Figure 6c shows a superposition of the two Ag sites (occupation 0.375), half-occupied O sites, and the tetrahedral framework atoms associated with a six-ring window. From the framework atoms, two reasonable framework conformations, which are geometrically equivalent and crystallographically related by a twofold axis, can be constructed. These correspond to two conformations of the six-ring window (shown in superposition in Fig. 6c). Similarly, there are two positions for the Ag^+ ion. From the two conformations of the six-ring window and from the two silver sites, two different arrangements of the Ag^+ ion in relation to the framework oxygens are possible. Figures 6d and 6e show these two types of Ag–O coordination for one of the two framework conformations. It is not possible to decide on the basis of diffraction data which of the two framework conformations belongs to which of the two positions of the Ag^+ ions. Both combinations lead to very similar silver–

oxygen coordinations. If the oxygen apices of the "six-ring crown" are turned toward the silver ion (Fig. 6d), the Ag–O distances are 2.375(6) and 2.899(6) Å; if the apices are turned away from the silver ion (Fig. 6e), the distances are 2.390(6) and 2.991(6) Å, respectively. In any case, the silver coordination is again threefold and very similar to the coordination at 298 K. The difference is that at 723 K the Ag^+ ion is situated slightly above the center of the triangle formed by the coordinating oxygen atoms, *i.e.*, it adopts a threefold coordination that seems to be more common that that observed at 298 K (see above). The distance of the silver ion from the center of the six-ring window (at fractional coordinates 0.25, 0.25, 0.25) is 0.31 Å, whereas in the low-temperature phase this distance amounts to 0.12 Å at 298 K and 0.10 Å at 623 K, respectively.

The Framework Conformation

The Al and Si atoms are ordered on the framework sites as indicated by the bond-length differences for positions 6*c* and 6*d* and as proved by ^{29}Si MAS NMR spectra (21).

In general, three different mechanisms are operative in the thermal expansion of sodalites. These are (T denotes a tetrahedral framework atom, *i.e.*, T is Al or Si here):

(a) changes in the T–O bondlengths;

(b) distortion of [TO_4] tetrahedra, *i.e.*, changes in the O–T–O angle;

(c) rotation of [TO_4] tetrahedra, *i.e.*, changes in the T–O–T angle.

Mechanism *a* usually has only small influence, as the T–O bonds are strong. Mechanism *b* can be measured by the angles α_{Al} and α_{Si}, *i.e.*, the O–Al–O and O–Si–O angles of those O–O edges that belong to the four-ring window of the sodalite framework. These edges differ from those lining the six-ring window (α'_{Al} and α'_{Si}) when tetragonal distortions occur (40). As the sodalite structure belongs to the class of collapsible frameworks according to the classification of Baur (41), the rotation of the framework tetrahedra around their local $\bar{4}$ axis (mechanism *c*) occurs in a cooperative manner. The degree of this tilting (mechanism *c*) of a sodalite framework is quantified by the tilt angle φ with $\varphi = 0°$ corresponding to the fully expanded framework (31, 40, 42). According to Taylor (43), this is the main parameter describing the framework conformation of sodalite structures. Hassan and Grundy (42) further differentiate between the rotations of the AlO_4 and SiO_4 tetrahedra, φ_{Al} and φ_{Si}. Under the assumption that $\alpha_{Al} = \alpha'_{Al}$ and $\alpha_{Si} = \alpha'_{Si}$, the framework geometry is directly related to the cell edge *a* of a compound via the tilt angle φ. According to Henderson and Taylor (31), Dempsey and Taylor (44), and Hassan and Grundy (42), the thermal expansion of sodalites can be rationalized and predicted in terms of the rotation of the tetrahedra.

In the case of ASS, φ_{Al} (φ_{Si}) drops from 15.8° (16.7°) at 298 K to 7.3° (8.3) at 623 K. Correspondingly, the Si–O–Al angle increases from 149° to 157°. These changes show that the dominant mechanism of thermal expansion in ASS is indeed the untilting of the framework. This untilting obviously reaches a limit at the transition temperature of 678 K. There are three possible reasons for this limit to occur:

(i) φ_{Al} approaches 0°, *i.e.*, the framework reaches the fully expanded state; however, φ_{Al} is still around 8° only about 50 K below the transition temperature and it seems unlikely that it will reach a value of 0° at the transition temperature.

(ii) According to Depmeier (40) there is a lower limit $\varphi_{min} > 0°$ to the tilt angle φ which is connected to an upper limit of the Si–O–Al angle, *i.e.*, the angle around the oxygen atom bridging two framework tetrahedra. For 1 : 1 aluminosilicate sodalites, this angle should not exceed a value of 160.5°. At 623 K, it has increased to 157°. Possibly, framework untilting stops at T_c; there would then be no further possibility of adapting the framework conformation to the space requirements of the Ag^+ ion, which increases with increasing temperature, causing the metal ions to move out of the six-ring window.

(iii) The oxygen coordination of Ag^+ as offered by the six-ring window changes from threefold planar at 298 K (d_{Ag-O}: 2.347(5) Å) to sixfold planar at 623 K with $d_{Ag-O} \geq 2.50$ Å. In view of the preference of the Ag^+ ion for small coordination numbers and short bond lengths, this coordination is not acceptable. The structural changes occurring during the phase transition however lead to a coordination (flat trigonal pyramid with silver at the apex) which is strongly preferred by Ag^+ ions.

In spite of similar lattice constants, similar framework conformations and similar coordination of Na^+ and Ag^+ in the structures of anhydrous sodium sodalite (structure refined at 675 K, 25) and of ASS (structure refined at 623 K in this work), no phase transition of the type described here for ASS has been observed for the sodium compound: The Na^+ ion, which tends to more ionic bonding, accepts the sixfold planar coordination in anhydrous sodium sodalite (23). This supports the view that *the phase transition is related to the special bonding properties and coordination demands of the Ag^+ ion and not to conformational changes of the framework that reach a limiting value.*

Above the phase transition, at 723 K, $\varphi_{Al}(\varphi_{Si})$ has increased again to 13.6° (14.0°) corresponding to a partly collapsed framework conformation similar to the one observed at 298 K. The possibility to collapse is provided by the space that the Ag^+ ions leave behind when moving out of the center of the six-ring window. The fact, that in

spite of a larger φ value the lattice parameter at 723 K (9.158(2) Å) is larger than that at 623 K (9.142(2) Å) stands in contradiction to the above-mentioned predicted proportionality between the cell edge and cos φ (42). The lattice constant can however be rationalized by taking into account the distortion of $[TO_4]$ tetrahedra (mechanism *b*, 40). In both refinements of the low-temperature phase of ASS, α_{Al} and α_{Si} are near the tetrahedral angle of 109.54°, *i.e.*, no significant distortions of the ideal tetrahedron geometrics occur. At 723 K, however, α_{Al} = 112.0° and α_{Si} = 112.9°, indicating a slight tetragonal distortion in the high-temperature phase. Using formula (19) from ref. (40), which relates the lattice parameter a to φ and α, lattice parameters can be calculated, which are identical to the measured ones (last row in Table 3). The reason for the occurrence of tetragonal distortions in the high-temperature form are not clear.

Due to the partial collapse of the framework at T_c, thermal expansion of the high-temperature phase is possibly, as in the low-temperature phase, dominated by framework untilting. Thus, thermal expansion can again best be described as quadratic. This contrasts to the observations made on sodalites containing large anions, *e.g.*, iodide sodalite and sulfate-containing sodalites (31). These species also exhibit discontinuities in their thermal expansion curves which are explained by the space requirements of the anions, which increases with increasing temperature. The nonframework cations then are pressed from off-center positions above the centers of the six-ring windows toward these centers. When they reach the center, no further framework untilting occurs and a discontinuity is observed in the thermal expansion. In these cases, however, the thermal expansion at temperatures above the discontinuity is linear (31).

A Scenario for Thermal Expansion and the Phase Transition in ASS

The following scenario for the thermal expansion and the phase transition in ASS can be developed on the basis of the present data and the preceding discussion: At 298 K, the Ag^+ ions of ASS are placed nearly in the center of the six-ring windows of the sodalite cages. With increasing temperature the framework untilts which leads to a continuous change in the coordination of the Ag^+ ions from threefold to sixfold planar, coupled with an increase in the shortest Ag–O distance from 2.347 to 2.50 Å. At the phase transition temperature, this coordination is no longer acceptable for the Ag^+ ion; it therefore leaves the center of the six-ring window, thus allowing the framework to collapse again. In this way, it gains a preferred coordinative environment. After that event, thermal expansion is quadratic again.

An intriguing question is whether at the transition temperature the Ag+ ions merely move away from the center of the six-ring window to one of the two available sites or whether a dynamic hopping of the Ag^+ ions between these two sites with a jump distance of 0.62 Å occurs. In the latter case, the framework should also dynamically change between its two conformations (corresponding to two sets of half-occupied O sites) and should in this way accompany the movements of the Ag^+ ions. The present X-ray structure refinement only gives a space and time-averaged superposition of all (partly) occupied atomic sites. Methods such as impedance spectroscopy, inelastic neutron scattering, or ^{109}Ag solid-state NMR probing the dynamic nature of the system have to be applied in order to elucidate this question. To us, the appreciable value of the transition enthalpy and the relatively high temperature at which the transition occurs suggest a dynamic process.

Comparison with Anhydrous Sodium Sodalite

In spite of the similarities of anhydrous sodium sodalite and ASS regarding the compositions, the lattice parameters (a = 9.122(1) Å at 675 K for anhydrous sodium sodalite (23), a = 9.142(2) Å at 623 K for ASS) and the crystal structures as determined at 675 and at 623 K, respectively, their phase transition behavior is strikingly different. As discussed above, the absence of the cubic–cubic transition of ASS for the sodium sodalite can be explained by the different bonding characteristics of Ag^+ and Na^+ ions. However, due to their cation-deficient character, both compounds $[A_3\square][Al_3Si_3O_{12}]$ are prone to undergo order–disorder transitions involving ordering of the cage cations: There are only three of them per cage which are spread over four tetrahedrally disposed sites. Ordering of the cage cations should transmit to the framework atoms and lead to strong distortions of the framework, resulting in a reduction of symmetry and the occurrence of peak splittings and/or superstructure reflections in the X-ray diffractogram. A phase transition with these characteristics was found only in the sodium sodalite at 523 K by DSC and variable-temperature X-ray diffraction (3). These methods, however, have not been able to detect a similar transition for ASS at temperatures down to 100 K. A possible explanation is based upon the recent observation that phase transitions in sodalite structures which involve cooperative ordering processes of guest species and conformational changes in the framework geometry are strongly influenced by the presence of defects and/or impurities and may be blocked even by low concentrations of defects or impurities (6). In the case of ASS, the observed partial decomposition may give rise to substantial concentrations of defects that block a possible order/disorder phase transition at lower temperatures.

ACKNOWLEDGMENTS

We thank Ch. Baerlocher and V. Gubser for the X-ray diffraction data acquisition on the Scintag powder diffractometer and G. Wildermuth for his assistance during the DSC measurements. Discussions with W. Depmeier were of great value. This work was supported by the Bundesminister für Forschung und Technologie Contract 03-FE3KON and by the Deutsche Forschungsgemeinschaft Contract Fe17-1.

REFERENCES

1. S. Assmann, P. Behrens, J. Felsche, G. van de Goor, P. Sieger, and G. Wildermuth, presented at the XVIth Congress and General Assembly of the International Union of Crystallography, Beijing, August 1993; abstract in *Acta Crystallogr. A Suppl.* **49**, 438 (1993).
2. M. Wiebcke, G. Engelhardt, J. Felsche, P. B. Kempa, P. Sieger, J. Schefer, and P. Fischer, *J. Phys. Chem.* **96**, 392 (1992).
3. P. Sieger, Ph.D. Thesis, Konstanz 1992; Hartung-Gorre-Verlag, Constance, Germany (ISBN 3-89191-593-4).
4. M. Wiebcke, P. Sieger, J. Felsche, G. Engelhardt, P. Behrens, and J. Schefer, *Z. Anorg. Allg. Chem.* **619**, 1321 (1993).
5. W. Depmeier, *Phys. Chem. Miner.* **15**, 419 (1988).
6. R. Melzer and W. Depmeier, *Ferroelectrics*, in press.
7. W. Depmeier, *Acta Crystallogr. B* **44**, 201 (1988).
8. W. Depmeier and W. Bührer, *Acta Crystallogr. B* **47**, 197 (1991).
9. J. W. Richardson, J. J. Pluth, J. V. Smith, W. J. Dytrych, and D. M. Bibby, *J. Phys. Chem.* **92**, 243 (1988).
10. P. Behrens, G. van de Goor, G. Engelhardt, and J. Felsche, presented at the IVth European Conference on Solid State Chemistry, Dresden, Sept. 7–9, 1992.
11. S. Luger, Ph.D. Thesis, Constance, 1987; Hartung-Gorre-Verlag, Constance, Germany (ISBN 3-89191-107-6).
12. A. Stein, P. M. Macdonald, G. A. Ozin, and G. D. Stucky, *J. Phys. Chem.* **94**, 6943 (1990).
13. G. A. Ozin, A. Stein, G. D. Stucky, and J. P. Godber, *in* "Inclusion Phenomena and Molecular Recognition" (J. L. Atwood, Ed.), p. 379. Plenum Press, New York, 1990.
14. A. Stein, G. A. Ozin, P. M. Macdonald, G. D. Stucky, and R. Jelinek, *J. Am. Chem. Soc.* **114**, 5171 (1992).
15. A. Stein, G. A. Ozin, and G. D. Stucky, *J. Am. Chem. Soc.* **114**, 8119 (1992).
16. A. Stein, G. A. Ozin, and G. D. Stucky, *J. Am. Chem. Soc.* **112**, 904 (1990).
17. A. Stein, M. Meszaros, P. M. Macdonald, G. A. Ozin, and G. D. Stucky, *Adv. Mater.* **3**, 306 (1991).
18. G. A. Ozin, A. Kuperman, and A. Stein, *Adv. Mater.* **1**, 69 (1989).
19. A. Stein, G. A. Ozin, and G. D. Stucky, *J. Soc. Photogr. Sci. Technol. Jpn.* **53**, 322 (1990).
20. G. D. Stucky and J. E. MacDougall, *Science* **247**, 669 (1990).
21. S. Aβmann, Ph.D. Thesis, Constance, 1992.
22. G. Engelhardt, J. Felsche, and P. Sieger, *J. Am. Chem. Soc.* **114**, 1173 (1992).
23. J. Felsche, S. Luger, and Ch. Baerlocher, *Zeolites* **6**, 367 (1986).
24. A. Schneider, S. Assmann, P. Behrens, M. Wiebcke, J. Felsche, and H. Mändar, presented at the 31st Discussion Meeting of the Deutsche Gesellschaft für Kristallographie, Bochum, March 1993; abstract in *Z. Kristallogr. Suppl.* **7**, 174 (1993).
25. Y. Kim and K. Seff, *J. Phys. Chem.* **82**, 1307 (1978).
26. P. A. Jacobs, J. B. Uytterhoeven, and H. K. Beyer, *J. Chem. Soc. Faraday Trans.* **75**, 56 (1979).
27. G. A. Ozin, M. D. Baker, and J. Godber, *J. Phys. Chem.* **88**, 4902 (1984).
28. J. Texter, R. Kellerman, and T. Gonsiorowski, *J. Phys. Chem.* **90**, 2118 (1986).
29. J. Ladell, A. Zagofsky, and S. Perlman, *J. Appl. Crystallogr.* **8**, 499 (1975).
30. Ch. Baerlocher, "The X-ray Rietveld System." Institut für Kristallographie und Petrographie der ETH Zürich, 1982.
31. C. M. B. Henderson and D. Taylor, *Phys. Chem. Miner.* **2**, 337 (1978).
32. L. R. Gellens, W. J. Mortier, and J. B. Uytterhoeven, *Zeolites* **1**, 11 (1981).
33. L. R. Gellens, W. J. Mortier, R. A. Schoonheydt, and J. B. Uytterhoeven, *J. Phys. Chem.* **85**, 2783 (1981).
34. L. R. Gellens, J. V. Smith, and J. J. Pluth, *J. Am. Chem. Soc.* **105**, 51 (1985).
35. M. Jansen, *Acta Crystallogr. B* **33**, 3584 (1977).
36. M. Jansen and K. Heidebrecht, *Z. Kristallogr.* **179**, 347 (1987).
37. G. Brachtel and M. Jansen, *Z. Anorg. Allg. Chem.* **478**, 13 (1981).
38. M. Jansen, M. Bortz and K. Heidebrecht, *J. Less-Common Met.* **161**, 17 (1990).
39. P. Behrens, *Solid State Commun.* **81**, 325 (1992).
40. W. Depmeier, *Acta Crystallogr. B* **40**, 185 (1984).
41. W. H. Baur, *J. Solid State Chem.* **97**, 234 (1992).
42. I. Hassan and H. D. Grundy, *Acta Crystallogr. B* **40**, 6 (1984).
43. D. Taylor, *Mineral. Mag.* **38**, 593 (1972).
44. M. J. Dempsey and D. Taylor, *Phys. Chem. Miner.* **6**, 197 (1980).